Microchimica Acta (2022) 189: 145
https://doi.org/10.1007/s00604-022-05178-9

ORIGINAL PAPER

Laser ablative TiO_2 and tremella-like $CuInS_2$ nanocomposites for robust and ultrasensitive photoelectrochemical sensing of let-7a

Cuiping Fu[1] · Xuefeng Wang[1] · Fumin Xue[2] · Peihua Zhu[3] · Weijia Zhou[1] · Shenguang Ge[1] · Jinghua Yu[3]

Received: 21 August 2021 / Accepted: 5 January 2022 / Published online: 16 March 2022

Abstract

A photoelectrochemical (PEC) biosensor based on a multiple signal amplification strategy was established for highly sensitive detection of microRNA (miRNA). TiO_2 was prepared on the surface of titanium sheet by laser etching to improve its stability and photoelectrical properties, and $CuInS_2$-sensitized TiO_2 was used to form a superior photoelectrical layer, which realized the initial signal amplification. The electron donor dopamine (DA) was modified to H2 as a signal regulator, which effectively increased the photocurrent signal. To further amplify the signal, an enzyme-free hybridization reaction was implemented. When target let-7a and fuel-DNA (F-DNA) were present, the base of H1 specifically recognized let-7a and forced dopamine@AuNPs-H2 away from the electrode surface. Subsequently, the end base of H1 specifically recognized F-DNA, and let-7a was replaced and recycled to participate in the next cycle. Enzyme-free circulation, as a multifunctional amplification method, ensured the recycling of target molecules. This PEC sensor for let-7a detection showed an excellent linear response from 0.5 to 1000 pM with a detection limit of 0.12 pM. The intra-batch RSD was 3.8% and the recovery was 87.74–108.1%. The sensor was further used for clinical biomolecular monitoring of miRNA, showing excellent quantitative detection capability.

Keywords Photoelectrochemical biosensor · Laser ablative TiO_2 · $CuInS_2$ · MicroRNA

Introduction

MicroRNA (miRNA) is a kind of endogenous, non-coding, small single-stranded RNA, with a size of about 22 nucleotides, which has a wide range of functions [1, 2]. The function of miRNA is to regulate the stability or transcriptional efficiency of the target gene miRNA and participate in different levels of life activities. It plays an indispensable role in regulating almost all important life processes, such as cell proliferation [3, 4], apoptosis, development, differentiation, and metabolism [5, 6]. It is closely related to the occurrence and development of tumor and cancer. In recent years, many studies have confirmed that miRNA plays an important role in the pathogenesis of cancer. A large number of miRNA genes are located in cancer-related genomic regions, which are altered in cancerous diseases. Therefore, miRNA is expected to become a therapeutic target for a variety of diseases, used to monitor and treat cancer [7, 8]. Therefore, accurate and rapid monitoring of miRNA is particularly crucial in understanding the pathogenesis and clinical diagnosis of the disease. Up to now, with the rapid advance of science and technology, many methods of detecting miRNA have emerged such as surface plasmon resonance [9, 10], microassay analysis [11], and bioluminescence assay [12]. However, these analytical methods usually have some limitations, such as complex operation, low sensitivity, and expensive instruments. Photoelectrochemical biosensors [13, 14], as an important branch of electrochemical biosensors, have

Cuiping Fu and Xuefeng Wang contributed equally to this work.

✉ Peihua Zhu
chm_zhuph@ujn.edu.cn

✉ Weijia Zhou
ifc_zhouwj@ujn.edu.cn

✉ Shenguang Ge
chm_gesg@163.com

[1] Collaborative Innovation Center of Technology and Equipment for Biological Diagnosis and Therapy in Universities of Shandong, Institute for Advanced Interdisciplinary Research, University of Jinan, Jinan 250022, People's Republic of China

[2] Shandong Analysis and Test Center, Qilu University of Technology (Shandong Academy of Sciences), Jinan 250014, People's Republic of China

[3] School of Chemistry and Chemical Engineering, University of Jinan, Jinan 250022, People's Republic of China

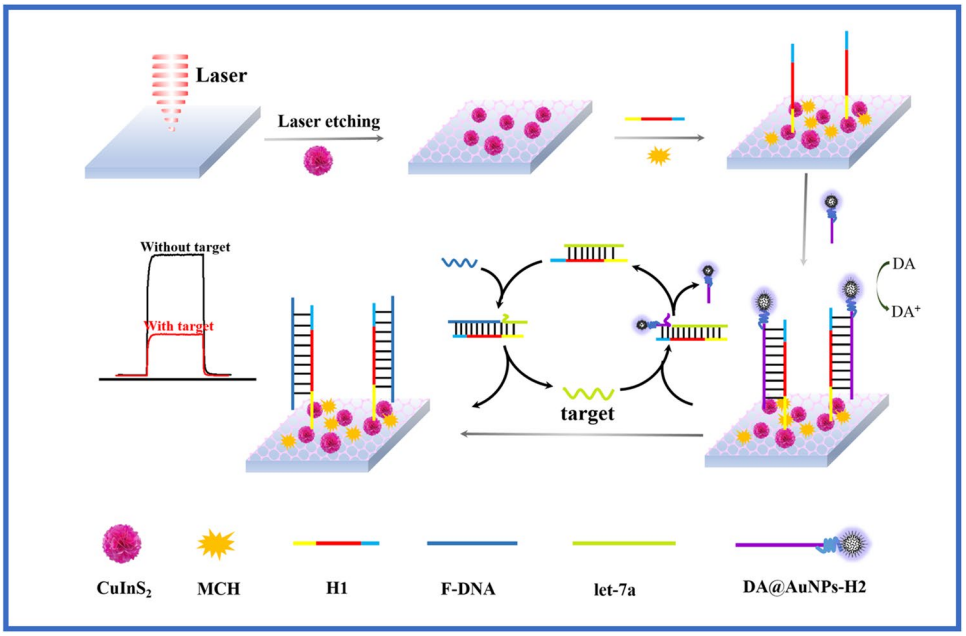

Scheme 1 Schematic of photoelectrochemical biosensor for detection of let-7a

attracted much attention in recent years due to their advantages of low background and high sensitivity.

Photoelectrochemical detection is a burgeoning and promising method for biological analysis [15–17]. On the one hand, photoelectric nanomaterials are very important for the construction of photoelectric chemical sensors [18–20]. On the other hand, due to the low abundance and easy degradation of miRNA in biological samples, it is urgent to improve the ultrasensitive detection of miRNA. Therefore, selecting the suitable photoelectric nanomaterials can improve the sensitivity of the sensor [21, 22]. As a typical photosensitive material, TiO_2 has been widely used on account of its excellent performance [23–25]. Nevertheless, the wide band gap of TiO_2 results in its ability to utilize only ultraviolet (UV) light in the UV range, which limits the application of TiO_2 in sensors [26, 27]. $CuInS_2$ is a classic I – III – VI ternary metal sulfide with a band gap of 1.5 eV, with a wide light absorption range and tunable band gap energy, causing wide attention [28]. $CuInS_2$ can be well coupled with TiO_2 and have excellent photoelectrochemical properties compared to other sensing materials, abundant charge transfer properties, and good energy level matching, so as to realize the directional flow of photo-generated carriers in the composite semiconductor, widen the absorption range of light, and improve the utilization ratio of excited light [29, 30]. However, TiO_2 nanomaterials prepared by conventional synthetic methods were difficult to achieve large-scale periodic preparation, long-term storage, good stability, and patterning electrode, so it was necessary to introduce new technologies. By using the significant local fast photothermal effect induced by focused laser, TiO_2 nanomaterials were prepared as the working electrode in a patterned way without interfering with the surrounding materials, replacing the conventional thermal treatment method for the nucleation and growth of nanomaterials. The resulting TiO_2 not only have better photoelectric properties, larger specific surface area, and more active sites, but also can be manufactured on a large scale and synthesized rapidly. Laser etching synthesis has the advantages of low energy consumption, simplicity, high scalability, mass production, and easy control [31], and has an inestimable application prospect in the field of electrochemistry.

Based on the above advantages, a new PEC sensing platform was developed based on the enzyme-free chain replacement reaction for highly sensitive detection of let-7a. As shown in Scheme 1, firstly, tremella-like $CuInS_2$ with the layered nano-flakes were modified onto the laser-etched TiO_2 flakes. The resulting $CuInS_2/TiO_2$ photoelectric layer had highly photogenerated carrier separation efficiency to visible light. Subsequently, H1 and the sealant 6-mercapto-1-hexanol (MCH) were introduced. Moreover, with dithiobis (succinimide propionate) (DSP) as the bridge, DA as the electron donor was chemically bonded to H2. DA@AuNPs-H2 could be used as a probe to amplify the signal of PEC biosensor. With the addition of the target and F-DNA, let-7a replaced H2. The F-DNA was hybridized to H1, and the target let-7a was released from the electrode surface to participate in the next cycle reaction. The signal amplification strategy used in this paper, which has no additional powering or enzymes involved, can better transport carriers and improve photoelectric conversion efficiency. Excitingly, the as-prepared TiO_2 and $CuInS_2$ indeed exhibited distinct PEC response. We greatly hope that this research would inspire interest in the fabrication and development of laser ablative

TiO_2 for sensitive and selective PEC bioanalysis in complex samples.

Experimental

Materials and apparatus

The materials and apparatus are described in the Supplementary Material.

Preparation of TiO_2 nanosheets

Firstly, the original titanium sheet was cleaned by ultrasonic treatment with diluted hydrochloric acid and ultrapure water for 30 min. The computer was connected with the laser system and the experimental parameters were set. The linear scanning mode with laser wavelength of 1064 nm, pulse duration of 100 ns in air atmosphere, average power of 10 W, and scanning speed of 2000 mms^{-1} was used for laser graphics. Subsequently, a size of 5 × 5 mm TiO_2 electrode was produced [32].

Preparation of tremella-like $CuInS_2$

Tremella-like $CuInS_2$ was prepared based on previous work [33]. Detailed steps are described in the Supplementary Material.

Preparation of DA@AuNPs-H2

Ten microliters of AuNPs was mixed with 20-μL 2 mM DSP aqueous solution, then 10 μL 10 mM DA was added to the mixed solution and shaken overnight. The obtained solution was mixed with 10 μL 100 nM H2 and placed on the shaker overnight to prepare DA@AuNPs-H2.

Fabrication of the enzyme-free PEC biosensor

A PEC biosensor mechanism for enzyme-free replacement cycle detection of microRNA is shown in Scheme 1. First of all, based on the advantages of laser etching synthesis, TiO_2 nanosheets (5 × 5 mm) were obtained by laser etching titanium sheets in air atmosphere. After that, the TiO_2 nanosheets were placed in ultrapure water for ultrasonic treatment. An aliquot of 20 μL of $CuInS_2$ was dripped onto TiO_2 nanosheets for 4 h at room temperature. Then, 10 μL H1 (10 μL) was incubated onto surface $CuInS_2$/TiO_2 at room temperature for 16 h. H1 was assembled on the modified electrode by sulfhydryl affinity and washed with ultrapure water to remove excess H1. The nonspecific binding site was sealed with 200 μL MCH (2.0 mM) for 40 min. Thereafter, DA@AuNPs-H2 (10 μL) was hybridized with H1. However, when the mixed solution of let-7a and F-DNA was incubated onto the-prepared electrode for 2 h at 4 °C, let-7a was recognized by the yellow fragment of H1 to hybridize with it, thus replacing DA@AuNPs-H2. Meanwhile, F-DNA was recognized by the blue part of H1 to replace let-7a; let-7a was released to participate in the next cycle. Accordingly, an enzyme-free circulating PEC biosensor was successfully constructed.

Results and discussions

Characterization of the laser etching TiO_2

The properties of a substance are closely related to the performance of photoelectrochemical biosensor. It is crucial for the performance of TiO_2 as the initial substrate to build a PEC biosensor. TiO_2 as the substance for working electrode was prepared by laser ablation. As can be seen from the scanning electron microscope (SEM) of Fig. 1a, the etched TiO_2 was arranged in a linear pattern with a width of 20 μm. This concave-convex arrangement allowed TiO_2 with more specific surface area and more sites, resulting in the amplification of photocurrent signal. The element mapping image (Fig. 1b) and energy-dispersive spectrum (Fig. 1c) of TiO_2 showed that Ti and O elements were evenly distributed, confirming the success of laser ablation of TiO_2. In order to prove the formation of TiO_2, X-ray diffraction (XRD) technique was used. As shown in Fig. 1d, the XRD diagram of TiO_2 clearly indicated that all of the peaks obtained by laser ablation was located at $2\theta = 20–80°$, which could be indexed from reflections (JCPDS card no. 34–0180) of TiO_2. The pattern showed a sharp diffraction peak, indicating high purity and high crystallinity. Finally, X-ray photoelectron spectroscopy (XPS) further provided powerful evidence of the successful laser ablation of TiO_2. The XPS spectra distinctly showed that the prepared TiO_2 contained Ti and O elements which were two distinct peaks, 459.15 eV and 464.85 eV (Fig. 1e), corresponding to Ti $2p_{3/2}$ and Ti $2p_{1/2}$, respectively. As shown in Fig. 1f, the O (1 s) peak situated at 530.55 eV was observed, which resulted from surface-bound oxygen-containing species. The results of XPS were consistent with those of XRD and confirmed that the high purity of TiO_2 was successfully prepared.

Characterization of $CuInS_2$

The surface morphology and structure of $CuInS_2$ nanomaterial were analyzed by SEM characterization. It was observed that $CuInS_2$ were tremella-like and have average diameters of 1.5 μm (Fig. 2a), which were composed of

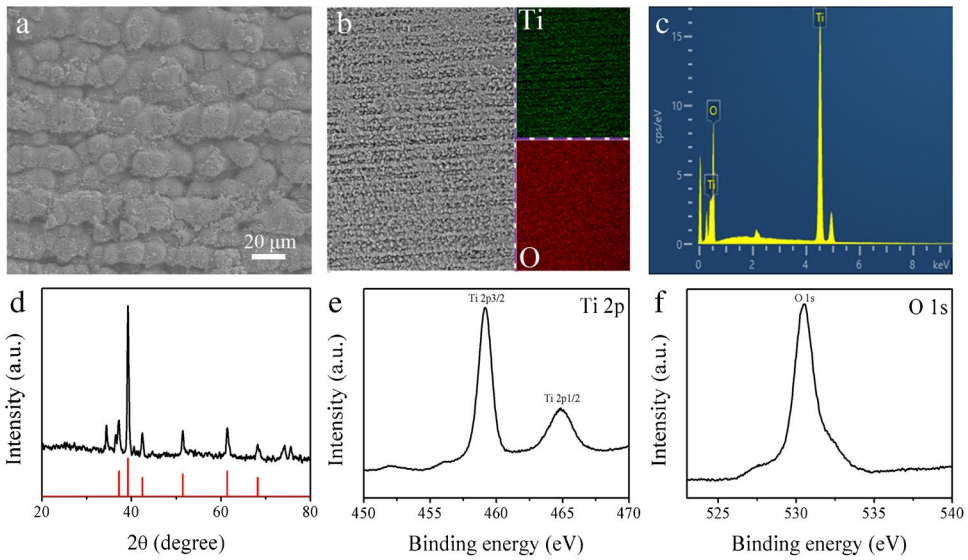

Fig. 1 SEM image (**a**), element mapping images of TiO_2 (**b**), and energy dispersive spectrum of TiO_2 (**c**). **d** XRD patterns of TiO_2, **e** XPS spectra of element of Ti, **f** XPS spectra of element of O

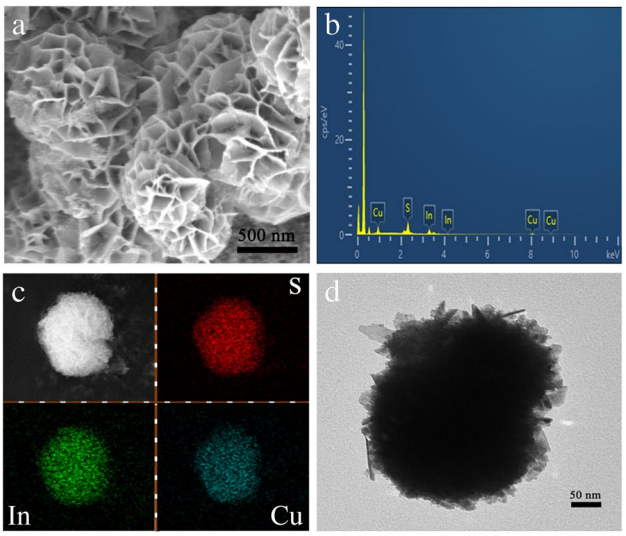

Fig. 2 SEM image of the $CuInS_2$ (**a**), EDS patterns of the $CuInS_2$ (**b**), the corresponding element mapping of S, In, and Cu respectively (**c**), TEM image of the $CuInS_2$ (**d**)

numerous slick nanosheets. This structure greatly increased the specific surface area. Figure 2b was the energy-dispersive spectroscopy (EDS) of tremella-like $CuInS_2$, from which the element peak of S, In, and Cu could be clearly observed. Moreover, the EDS mapping results showed the compact location of S, In, and Cu distributed on tremella-like $CuInS_2$ as shown in Fig. 2c. In addition, as shown in in Fig. 2d, the TEM image of tremella-like $CuInS_2$ showed that there were many thin sheets on the edge of it, and it was concluded that it was composed of thin nanosheets with a large surface area. And the XPS spectra, XRD spectra, and Raman spectra of $CuInS_2$ were described in supplementary materials (Fig. S1). The above results proved that the tremella-like $CuInS_2$ were synthesized successfully.

EIS and PEC characterization of the fabricated biosensor

To demonstrate the manufacturing process of PEC biosensor, the electrochemical characterization of the stepwise-modified electrode was executed by electrochemical impedance spectroscopy (EIS) in 5.0 mM $[Fe(CN)_6]^{3-/4-}$ solution containing 0.1 M KCl. The charge transfer resistance (R_{et}) corresponds to the semicircle diameter in the higher part of the EIS diagram, and the change in resistance is related to the electrode modification. Figure 3a shows the electrochemical impedance diagram of the modified electrode, and the illustration was the corresponding equivalent circuit diagram. The working electrode of unmodified TiO_2 sheet showed a small semicircle (curve a). After $CuInS_2$ was assembled on the electrode, the R_{et} value increased obviously due to the weak conductivity of the semiconductor (curve b). When H1 was fixed to the modified electrode, the R_{et} value began to increase (curve c). After sealing the electrode with MCH, the R_{et} value continued to increase (curve d), which was due to the fact that the blocking agent hindered the electron transfer on the surface of the electrode. When the electrode (MCH/H1/$CuInS_2$/TiO_2) was modified by the DA-DSP@AuNPs-H2, the R_{et} value was distinctly increased (curve e) in virtue of the non-conductivity of the biomolecule and the organic molecule. In the end, when the modified electrode was incubated with the mixed solution of F-DNA and let-7a, the R_{et} value declined (curve f). The EIS results indicated that the PEC biosensor was successfully fabricated. To

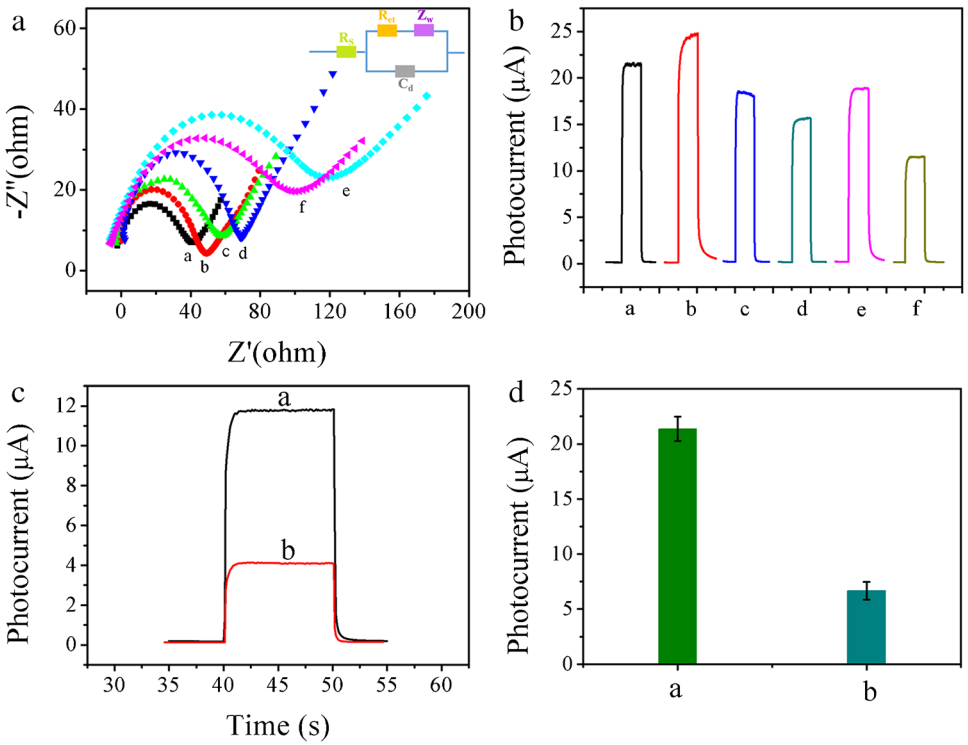

Fig. 3 **a** EIS characterizations and **b** photocurrent responses of the stepwise modified electrodes: (a) TiO_2, (b) $CuInS_2$/TiO_2, (c) H1/$CuInS_2$/TiO_2, (d) MCH/H1/$CuInS_2$/TiO_2, (e) DA@AuNPs-H2/MCH/H1/$CuInS_2$/TiO_2 (f) F-DNA/MCH/H1/$CuInS_2$/TiO_2. The EIS measurement was performed in 5 mM $[Fe(CN)_6]^{3-/4-}$ solution containing 0.1 M KCl. Photocurrent detection was carried out in PBS solution (PH 7.4) containing 0.01 M DA. **c** Photocurrent responses of (a) DA@AuNPs-H2/MCH/H1/$CuInS_2$/TiO_2, (b) F-DNA/MCH/H1/$CuInS_2$/TiO_2 in PBS solution (PH 7.4). **d** Photocurrent responses of the different methods to obtain electrodes: (a) laser etching of TiO_2, (b) TiO_2/GCE. Error bars, S.D., $n = 3$

verify the successful construction of the PEC biosensor, the photocurrent response monitoring is shown in Fig. 3b. The experiment was carried out in a PBS solution (pH 7.4) containing 0.01 M DA. The photocurrent signal produced by laser-etched TiO_2 film under light is shown in the Fig. 3b (curve a). When $CuInS_2$ was modified on TiO_2, the photocurrent signal increased significantly (curve b). On the one hand, the unique structure of tremella-like $CuInS_2$ exhibited photoactivity enhancement under a visible-light irradiation. On the other hand, TiO_2 and $CuInS_2$ can well match energy levels, thus promoting electron transfer and improving photocurrent signal. These two advantages resulted in high photoelectric conversion efficiency. After the immobilization of H1 and MCH, the photocurrent response decreased (curves c, d), which may be attributed to the fact that biomolecules and organic molecules hindered the transfer of electrons, which was not conducive to the separation of photogenerated electron holes. However, the photocurrent response increased followed by the DA@AuNPs-H2 immobilization (curve e), which was attributed to the change of DA to provide electrons under visible light irradiation, introducing an electron donor as a capture body for light-generated holes. When F-DNA and let-7a were recombined on the modified electrode, the photocurrent signal decreased (curve f). The photocurrent response experiment proved the successful construction of the biosensor.

The DA acted as an electron donor to signal amplification through availably inhibiting the electron – hole recombinant. To clarify the contribution of DA to signal amplification, a set of tests was implemented in PBS solution (pH 7.4). As can be seen from Fig. 3c, after immersing DA@AuNPs-H2/MCH/H1/$CuInS_2$/TiO_2 electrode in PBS solution (pH 7.4), DA as an electron donor provided electrons to the structure of $CuInS_2$/TiO_2 to produce holes under light excitation; thus, the photocurrent was enhanced (curve a). However, the photocurrent response evidently decreased after modifying the mixed solution with let-7a and F-DNA (curve b). The let-7a and F-DNA hybridized with the H1. DA@AuNPs-H2 was replaced by let-7a and hybridized with H1, and then let-7a was replaced by F-DNA. The hybridization process caused the release of DA@AuNPs-H2 from the electrode surface, so the photocurrent signal was reduced. The experimental results showed that the signal amplification strategy was feasible.

The photoelectric properties of substrate materials are particularly important for the construction of photoelectrochemical biosensors. The photocurrent responses of TiO_2 nanomaterials obtained by different methods were carried out. TiO_2 materials were prepared by hydrothermal method and the photocurrent of TiO_2/GCE was measured according to the reported literature [34, 35]. As shown in the Fig. 3d, under the same conditions, the photocurrent signal of TiO_2 directly as electrode obtained by laser etching was larger than that of TiO_2 modified by hydrothermal method on glassy carbon electrode. Therefore, TiO_2 obtained by laser

ablation is selected as the electrode of photoelectrochemical biosensor.

Photoelectrochemical detection for target RNA

Under the best conditions (see supplementary material), the linear relationship of the target let-7a concentration toward PEC signal was studied. Figure 4a displays the photocurrent responses measured at different concentration of let-7a. With the concentration of let-7a increasing, more DA@AuNPs-H2 was replaced by let-7a and away from the electrode surface, leading to a decrease in photocurrent signal. As seen from Fig. 4b, there was a good linear relationship between the photocurrent and the logarithm value of let-7a concentration in the range from 0.5 to 1000 pM. The linear regression equation was $I = 21.01 - 1.867\log C_{let\text{-}7a}$, with a correlation coefficient of 0.994. The limit of detection (LOD) was estimated to be 0.12 pM ($S/N = 3$). Compared with many reported results of study let-7a (Table 1), the detection limit of this PEC sensor is better than them.

Stability, reproducibility, and selectivity of the PEC biosensor

It is vital for PEC biosensor to evaluate the performance by the stability. As a part of PEC biosensor, the stability of the $CuInS_2/TiO_2$ electrode was also very important during the measurement. Under the condition of repeated light irradiation in PBS with DA, the stability of the sensor was detected by testing the stability of the photocurrent signal of $CuInS_2/TiO_2$ electrode. As could be seen from Fig. 5a, the produced photocurrents on the modified electrode were almost unchanged in "on – off" runs by controlling the light irradiation switch. These results indicated that the prepared photosensitive materials had good stability and could be used to construct PEC sensors. In addition, under the same other conditions, the prepared sensing electrodes were stored at 4 °C and measured at an interval of 1 week. Figure 5b illustrates that the photocurrent response kept at 88.7% of its original response within 4 weeks. All results demonstrated the excellent stability of the designed biosensor.

Table 1 Performance of miRNA detection contrasted with other works

Analytical method	Detection limit	Linear range	Refs[a]
Electrochemistry	1 pM	1–800 pM	1
Fluorescence	0.4 pM	0.5–500 pM	2
Fluorescence	0.78 nM	1.56–400 nM	3
Colorimetry	21.7 pM	50–10 nM	4
Mesoporous silica/PtNps nanomaterials	2.56 nM	5–100 nM	5
PEC	0.12 pM	0.5–1000 pM	This work

[a]References, see the Supplementary Material

The reproducibility of PEC biosensor was proved by evaluating the relative standard deviation (RSD) of intra-batch and inter-batch. In the process, we used the let-7a at concentrations of 0. 1, 0. 5, and 1 nM to evaluate reproducibility. Figure 5c presents that the RSD value of intra-batch was 3.8%, 5.6%, 4.5%. The sensor RSD value of inter-batch was 7.8%, 6.6%, 7.5%, respectively. Therefore, the proposed PEC biosensor had a good reproducibility.

Selectivity is one of the most important properties for a biosensor. Whether in point-of-care testing or clinical applications, the high selectivity of biosensors is very significant. Under the best experimental condition, the possible disruptors, such as miR-21, let-7e, let-7i, and let-7a, were incubated with biosensors. As could be seen from Fig. 5d, compared to the let-7a, high current responses of the above compounds were observed, which was in agreement with of the blank. It seemed beyond dispute that with the decrease of paired bases, the chain replacement was difficult to react, and the photocurrent signal had no obvious change. Hence, the experimental results suggested that the designed biosensor had a better selectivity of the target. However, this method still has the limitation that it cannot detect multiple objects simultaneously.

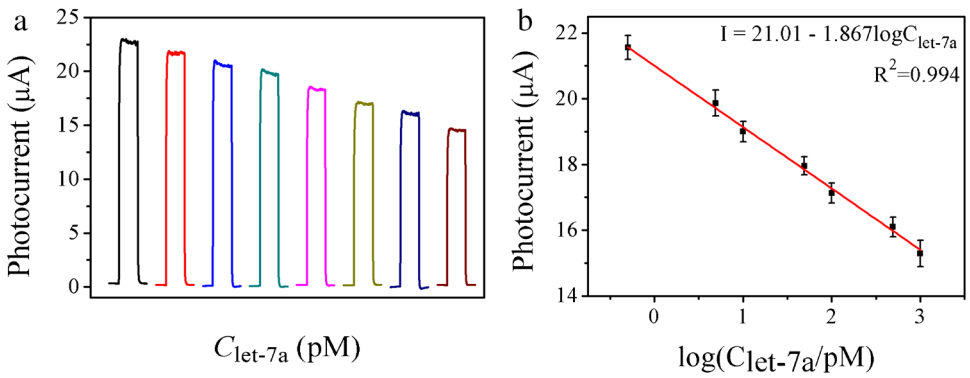

Fig. 4 **a** Photocurrent responses of the PEC biosensor at various concentrations of let-7a in 6 mL of PBS (pH 7.4) containing 0.01 M DA (0 pM, 0.5 pM, 5 pM, 10 pM, 50 pM, 100 pM, 500 pM, 1000 pM). **b** Relationship between the peak current value and let-7a concentration. Error bars, S.D., $n = 3$

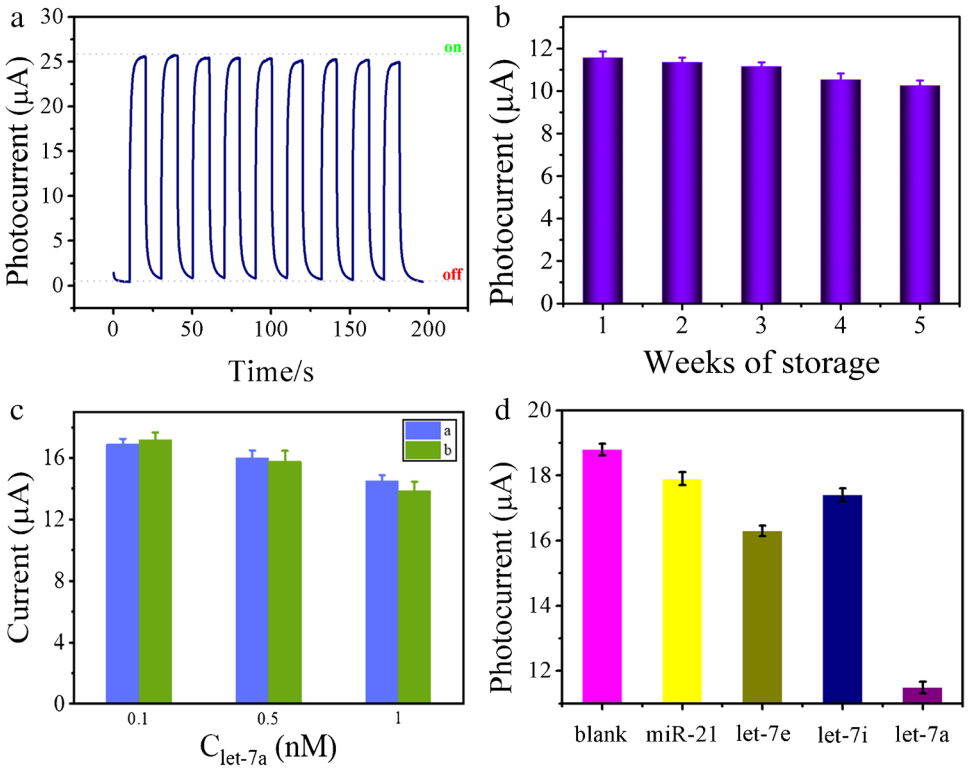

Fig. 5 **a** The stability of the $CuInS_2$ nanoflowers modified TiO_2 electrode and **b** the proposed PEC biosensor in the refrigerator (4 °C). **c** The photocurrents response of PEC biosensor intra (a) and inter (b) the groups. **d** Photocurrent responses of the PEC biosensor with different sequences of target (10 μL, 0.1 μM): blank, miR-21 (0.5 μM), let-7e (0.5 μM), let-7i (0.5 μM), and let-7a (0.1 μM). Error bars, S.D., $n=3$

Conclusions

A multiple signal amplification PEC biosensor was successfully established for ultrasensitive detection of microRNA with laser ablative TiO_2 and tremella-like $CuInS_2$ nanocomposites. This sensor had the advantages of ease operation, high sensitivity, strong anti-interference ability, which were attributed to the following points: (1) TiO_2 obtained by laser etching as the substance of the experiment had a more stable photocurrent. (2) $CuInS_2$ could not only sensitize TiO_2 electrode, but also significantly enhanced photocurrent signal because of its high visible light absorption capacity, which made the PEC biosensor bright in the way of detecting biomolecules. (3) The electron donor DA as a signal amplifier was assembled with a carefully designed H2 (DSP@AuNPs-H2) and applied to a PEC biosensor by base specific recognition. Meanwhile, $CuInS_2$ can consume electron donor DA efficiently under visible light irradiation because of its excellent light absorption ability. In addition, this highly specific enzyme-free hybridization avoided the effects of the introduction of other enzymes and enabled the target to be recycled. Although this method cannot detect multiple targets simultaneously, it provides a new PEC pathway for the detection of biomolecules with high sensitivity and selectivity.

Supplementary Information The online version contains supplementary material available at https://doi.org/10.1007/s00604-022-05178-9.

Funding This work was supported by the National Natural Science Foundation of China (22074053, 21775055, 21874055); A project of Shandong Province Higher Educational Youth Innovation Science and Technology Program (2020GXRC047, 2019KJC016); The Project of "20 items of University" of Jinan (2018GXRC001); the Taishan Scholars program and Case-by-Case Project for Top Outstanding Talents of Jinan.

Declarations

Conflict of interest The authors declare no competing interests.

References

1. Zhang J, Chen C, Fu H, Yu J, Sun Y, Huang H (2020) MicroRNA-125a-Loaded polymeric nanoparticles alleviate systemic lupus erythematosus by restoring effector/regulatory T cells balance. ACS Nano 14:4414–4429
2. Wang SF, Wu CJ, Luo JJ, Luo XL, Yuan R, Yang X (2020) Target-triggered configuration change of DNA tetrahedron for SERS assay of microRNA 122. Microchim Acta 187:460
3. Ren K, Zhang Y, Zhang X, Liu Y, Yang M, Ju H (2018) In situ siRNA assembly in living cells for gene therapy with microRNA triggered cascade reactions templated by nucleic acids. ACS Nano 12:10797–10806
4. Mozneb M, Mirtaheri E, Sanabria AO, Li CZ (2020) Bioelectronic properties of DNA, protein, cells and their applications for diagnostic medical devices. Biosens Bioelectron 167:112441
5. Zhao XP, Liu FF, Hu WC, Younis MR, Wang C, Xia XH (2019) Biomimetic nanochannel-ionchannel hybrid for ultrasensitive and label-free detection of microRNA in cells. Anal Chem 91:3582–3589

6. Liu J, Cui M, Zhou H, Yang W (2017) DNAzyme based nanomachine for in situ detection of microRNA in living cells. ACS Sens 2:1847–1853
7. Luo X, Li Z, Wang G, He X, Shen X, Sun Q (2017) MicroRNA-Catalyzed cancer therapeutics based on DNA-Programmed nanoparticle complex. ACS Appl Mater Interfaces 9:33624–33631
8. Bertucci A, Kim KH, Kang J, Zuidema JM, Lee SH (2019) Tumor-Targeting, microRNA-silencing porous silicon nanoparticles for ovarian cancer therapy. ACS Appl Mater Interfaces 11:23926–23937
9. Da P, Li W, Lin X, Wang Y, Tang J, Zheng G (2014) Surface plasmon resonance enhanced real-time photoelectrochemical protein sensing by gold nanoparticle-decorated TiO_2 nanowires. Anal Chem 86:6633–6639
10. Hu F, Xu J, Chen Y (2017) Surface plasmon resonance imaging detection of sub-femtomolar microRNA. Anal Chem 89:10071–10077
11. Sun X, Wang H, Jian Y, Lan F, Zhang L, Liu H (2018) Ultrasensitive microfluidic paper-based electrochemical/visual biosensor based on spherical-like cerium dioxide catalyst for miR-21 detection. Biosens Bioelectron 105:218–225
12. Li XQ, Deng L, Ma FH, Yang MH (2020) A luminous off-on probe for the determination of 2,6-pyridinedicarboxylic acid as an anthrax biomarker based on water-soluble cadmium sulfide quantum dots. Microchim Acta 187:287
13. Blidar A, Trashin S, Carrion EN, Gorun SM, Cristea C, De Wael K (2020) Enhanced photoelectrochemical detection of an analyte triggered by its concentration by a singlet oxygen-generating fluoro photosensitizer. ACS Sens 5:3501–3509
14. Zhang XY, Han L, Yu LD, Wang XH, Ling Y, Li NB (2021) Crystal violet-sensitized direct z-scheme heterojunction coupled with a g-wire superstructure for photoelectrochemical sensing of Uracil-DNA glycosylase. ACS Appl Mater Interfaces 13:15881–15889
15. Yuan Y, Hu T, Zhong X, Zhu M, Chai Y, Yuan R (2020) Highly sensitive photoelectrochemical biosensor based on quantum dots sensitizing Bi_2Te_3 nanosheets and DNA-Amplifying strategies. ACS Appl Mater Interfaces 12:22624–22629
16. Wang B, Mei LP, Ma Y, Xu YT, Ren SW, Cao JT (2018) Photoelectrochemical-chemical-chemical redox cycling for advanced signal amplification: proof-of-concept toward ultrasensitive photoelectrochemical bioanalysis. Anal Chem 90:12347–12351
17. Meng YC, Wang SS, Zhao JK, Hun X (2020) Photoelectrochemical aptasensor with low background noise. Microchim Acta 187:622
18. Wang S, Zhao J, Zhang Y, Yan M, Zhang L, Ge S (2019) Photoelectrochemical biosensor of HIV-1 based on cascaded photoactive materials and triple-helix molecular switch. Biosens Bioelectron 139:111325
19. Zhao CQ, Zhou J, Wu KW, Ding SN, Xu JJ, Chen HY (2020) Plasmonic enhanced gold nanoclusters-based photoelectrochemical biosensor for sensitive alkaline phosphatase activity analysis. Anal Chem 92:6886–6892
20. Song Z, Fan GC, Li Z, Gao F, Luo X (2018) Universal design of selectivity-enhanced photoelectrochemical enzyme sensor: integrating photoanode with biocathode. Anal Chem 90:10681–10687
21. Qin XF, Geng LP, Wang QQ, Wang Y (2019) Photoelectrochemical aptasensing of ofloxacin based on the use of a TiO_2 nanotube array co-sensitized with a nanocomposite prepared from polydopamine and Ag_2S nanoparticles. Microchim Acta 186:430
22. Wang Y, Bian F, Qin XF, Wang QQ (2018) Visible light photoelectrochemical aptasensor for chloramphenicol by using a TiO_2 nanorod array sensitized with Eu(III)-doped CdS quantum dots. Microchim Acta 185:161
23. Gao B, Zhao X, Liang Z, Wu Z, Wang W, Han D (2021) CdS/TiO_2 nanocomposite-based photoelectrochemical sensor for a sensitive determination of nitrite in principle of etching reaction. Anal Chem 93:820–827
24. Beketova D, Motola M, Sopha H, Michalicka J, Cicmancova V, Dvorak F (2020) One-Step decoration of TiO_2 nanotubes with Fe_3O_4 nanoparticles: synthesis and photocatalytic and magnetic properties. ACS Appl Nano Mater 3:1553–1563
25. Dashtian K, Ghaedi M, Hajati S (2019) Photo-sensitive $Pb_5S_2I_6$ crystal incorporated polydopamine biointerface coated on nanoporous TiO_2 as an efficient signal-on photoelectrochemical bioassay for ultrasensitive detection of Cr(VI) ions. Biosens Bioelectron 132:105–114
26. Haidry AA, Xie L, Wang Z, Zavabeti A, Li Z, Plecenik T (2019) Remarkable improvement in hydrogen sensing characteristics with Pt/TiO_2 interface control. ACS Sens 4:2997–3006
27. Chen Y, Zhang S, Dai H, Hong Z, Lin Y (2020) A multiple mixed TiO_2 mesocrystal junction based PEC-colorimetric immunoassay for specific recognition of lipolysis stimulated lipoprotein receptor. Biosens Bioelectron 148:111809
28. Chang S, Zhao Y, Tang J, Bai Z, Zhao L, Zhong H (2020) Balanced carrier injection and charge separation of $CuInS_2$ quantum dots for bifunctional light-emitting and photodetection devices. J Phy Chem C 124:6554–6561
29. Shen F, Que W, Liao Y, Yin X (2011) Photocatalytic activity of TiO_2 nanoparticles sensitized by $CuInS_2$ quantum dots. Ind Eng Chem Res 50:9131–9137
30. Han M, Jia J, Wang W (2016) Pulsed laser deposition of a Bi_2S_3/$CuInS_2$/TiO_2 cascade structure for high photoelectrochemical performance. RSC Adv 6:70952–70959
31. Yuan H, Liu F, Xue G, Liu H, Wang Y, Zhao Y (2021) Laser patterned and bifunctional Ni@N-doped carbon nanotubes as electrocatalyst and photothermal conversion layer for water splitting driven by thermoelectric device. Appl Catal B 283:119647–119656
32. Zhao LL, Liu Z, Chen D, Liu F, Yang ZY, Li X, Yu HH, Liu H, Zhou WJ (2021) Laser synthesis and microfabrication of micro/nanostructured materials toward energy conversion and storage. Nano Micro Lett 2311–6706
33. Zhang F, Chen Y, Zhou W, Ren C, Gao H, Tian G (2019) Hierarchical SnS_2/$CuInS_2$ nanosheet heterostructure films decorated with C_{60} for remarkable photoelectrochemical water splitting. ACS Appl Mater Interfaces 11:9093–9101
34. Li HB, Li J, Xu Q, Hu XY (2011) Poly(3-hexylthiophene)/TiO_2 nanoparticle-functionalized electrodes for visible light and low potential photoelectrochemical sensing of organophosphorus pesticide chlopyrifos. Anal Chem 83:9681–9686
35. Li HB, Li J, Xu Q, Hu XY (2011) Co_3O_4 -Au polyhedron mimic peroxidase- and cascade enzyme-assisted cycling process-based photoelectrochemical biosensor for monitoring of miRNA-141. Chem Eng J 406:126892